# NUMERICAL MODELING OF TSUNAMI GENERATION BY SUBMARINE AND SUBAERIAL LANDSLIDES

ISAAC V. FINE[1, 2, 4], ALEXANDER B. RABINOVICH[2, 3, 4], RICHARD E. THOMSON[4], and EVGUENI A. KULIKOV[2, 3, 4]
[1] *Heat and Mass Transfer Institute, Minsk, Belarus*
[2] *International Tsunami Research, Inc., Sidney, BC, Canada*
[3] *P.P. Shirshov Institute of Oceanology, Moscow, 117851 Russia*
[4] *Institute of Ocean Sciences, Sidney, BC, Canada*

## Abstract

Recent catastrophic tsunamis at Flores Island, Indonesia (1992), Skagway, Alaska (1994), Papua New Guinea (1998), and İzmit, Turkey (1999) have significantly increased scientific interest in landslides and slide-generated tsunamis. Theoretical investigations and laboratory modeling further indicate that purely submarine landslides are ineffective at tsunami generation compared with subaerial slides. In the present study, we undertook several numerical experiments to examine the influence of the subaerial component of slides on surface wave generation and to compare the tsunami generation efficiency of viscous and rigid-body slide models. We found that a rigid-body slide produces much higher tsunami waves than a viscous (liquid) slide. The maximum wave height and energy of generated surface waves were found to depend on various slide parameters and factors, including slide volume, density, position, and slope angle. For a rigid-body slide, the higher the initial slide above sea level, the higher the generated waves. For a viscous slide, there is an optimal slide position (elevation) which produces the largest waves. An increase in slide volume, density, and slope angle always increases the energy of the generated waves. The added volume associated with a subaerial slide entering the water is one of the reasons that subaerial slides are much more effective tsunami generators than submarine slides. The critical parameter determining the generation of surface waves is the Froude number, *Fr* (the ratio between slide and wave speeds). The most efficient generation occurs near resonance when *Fr* = 1.0. For purely submarine slides with $\rho_2 \le 2.0$ g·cm$^{-3}$, the Froude number is always less than unity and resonance coupling of slides and surface waves is physically impossible. For subaerial slides there is always a resonant point (in time and space) where *Fr* = 1.0 for which there is a significant transfer of energy from a slide into surface waves. This resonant effect is the second reason that subaerial slides are much more important for tsunami generation than submarine slides.

.

A. C. Yalçıner, E. Pelinovsky, E. Okal, C. E. Synolakis (eds.),
Submarine Landslides and Tsunamis 69-88.

## 1. Introduction

Submarine landslides, slumps, rock falls, and avalanches may produce catastrophic tsunami waves in coastal areas of the World Ocean. Although landslide generated tsunamis are much more localized than seismically generated tsunamis, they can produce destructive coastal run-up and cause severe damage to coastal emplacements [1, 13]. Recent catastrophic tsunamis at Flores Island (1992), Papua New Guinea (1998), and İzmit, Turkey (1999) apparently originated with local landslides triggered by earthquakes [2, 3, 4, 5]. These events, as well as the non-seismic catastrophic event in 1994 in Skagway Harbor, Southeast Alaska [6, 7, 8], have significantly increased scientific interest in landslides and slide-generated tsunamis.

Submarine landslides are ineffective at tsunami generation compared with subaerial slides [9]. Subaerial slides displace a considerable volume of water at relatively high speed as they slide into the water from the foreslope. The famous event of July 10, 1958 in Lituya Bay, Southeast Alaska was initiated by a subaerial rockslide at the head of the bay that caused a giant tsunami which impacted the sides of the inlet to a height of 525 m [10, 11]. The destructive Skagway event of November 3, 1994 was associated with a subaerial slide component which generated a series of large amplitude waves, estimated by eyewitnesses to have heights of 5-6 m in the harbor and 9-11 m at the shoreline [11, 6, 8]. Because the efficiency of tsunami generation is inversely proportional to the water depth, subaerial slides are particularly effective wave generators. *Raichlen et al.* [12], using laboratory modeling, examined the 1994 Skagway tsunami and demonstrated that the subaerial component of the slide caused a significant increase in the slide-generated wave amplitudes.

Numerical modeling of tsunamis caused by submarine slides and slumps is a much more complicated problem than simulation of seismically-generated tsunamis. The durations of the slide deformation and propagation are sufficiently long that they affect the characteristics of the surface waves. As a consequence, coupling between the slide body and the surface waves must be considered. Moreover, the landslide shape changes significantly during slide movement, causing the slide to modify the surface waves it has generated. *Jiang and LeBlond* [1,13] appear to have been the first to formulate models that account for all submarine landslides effects, including the coupling of the landslide and associated surface waves. We have corrected minor errors in the governing equations of the three-dimensional viscous-slide shallow-water model proposed by *Jiang and LeBlond* [1] (herein JLB94) and generalized the model to include arbitrary bottom topography (see [14] and [15] for details). Customized versions of this model were used to simulate the 1999 PNG tsunami [4, 16, 17] and the tsunami caused by the slumping of the Nice harbour extension (1979) [18].

The principal advantage of our extended model over the JLB94 model is the inclusion of a subaerial component of the slide. The main problem concerning the numerical modeling of subaerial slides is that 'wet' and 'dry' areas change during the slide/wave motions, so that there are variable boundaries between these areas. Only a few papers [19, 20] deal with this problem. Here, we have effectively bypassed the moving boundary problem and successfully used our model to simulate subaerial tsunamis for realistic bathymetry and coastline geometry, with application to the 1966 and 1994 tsunamis in Skagway Harbor, Alaska [15]. We also made similar modifications to the commonly used rigid-body (frictional) shallow-water slide model [21, 22]. The main purposes of the present

study are to examine the influences of subaerial landslides on tsunami wave generation and to compare the tsunami generation efficiency of viscous and rigid-body slide models. We also examine the influence of various slide parameters, such as slope angle, slide position, water depth, and friction, on surface wave generation.

## 2. Governing Equations and Model Description

Surface wave generation by a moving slide is affected by the water depth, gravity, and fundamental characteristics of the slide [1, 13]. The principal mechanism for energy transfer from the slide motion to the surface waves, water displacement, is readily incorporated using the long-wave (shallow-water) approximation [22]. The main assumptions for the present models (viscous and rigid-body) are the following:

(1) The surface waves and slides satisfy the long-wave (hydrostatic) approximation, implying that the wavelength of the water waves is much greater than the water depth, and that the width and length of the viscous slide is much greater than the slide thickness.

(2) The viscous slide is an incompressible, isotropic, laminar, quasi-steady viscous fluid; the viscous regime is rapidly reached in any failure and in the steady-state regime, the horizontal velocities have a parabolic vertical profile.

(3) The rigid-body slide moves as a non-deformable body with given friction.

(4) The seawater is an incompressible inviscid fluid.

We use standard Cartesian coordinates *x*, *y*, *z*, with *z* measured vertically upward. For time $t$, the upper (water) layer consists of seawater with density $\rho_1$, surface elevation $\eta(x, y; t)$, and horizontal velocity $\mathbf{u}$ with components *u* and *v* (Figure 1a). The lower layer consists of viscous sediments (or rigid body) having density $\rho_2$, dynamic viscosity $\mu$ (or friction coefficient *k* in case of a rigid body), and horizontal velocity $\mathbf{U}$ with components *U* and *V*. Both the slope and the slide have small angles, so the motion is essentially horizontal. The slide is bounded by an upper surface $z = -h(x, y; t)$ and the seabed surface $z = -h_s(x, y)$, giving the slide thickness as $D(x, y; t) = h_s(x, y) - h(x, y; t)$.

A schematic of the computational domain for a landslide with a subaerial component is presented in Figure 1. The domain consists of four zones: (1) The *dry* coastal area, $D$; (2) the *dry* portion of the slide, $S_D$, corresponding to the subaerial part of the slide; (3) the *wet* portion of the slide, $S_W$, corresponding to the submarine part of the slide; and (4) the *water*, $W$. The numerical model must account for the time-varying changes in the areas and locations of these zones.

### 2.1. VISCOUS SLIDE

Our purpose is to construct the non-linear, vertically integrated Navier-Stokes equations for the landslide. We assume that the landslide occupies a domain from $z = -h_s(x, y)$ to $D(x, y; t) = h_s(x, y) - h(x, y; t)$. Following JLB94, we assume that the landslide rapidly reaches a steady shape so that we can use a locally parabolic approximation in the vertical to describe the horizontal velocities, $U_m(x, y, z; t)$ and $V_m(x, y, z; t)$; specifically,

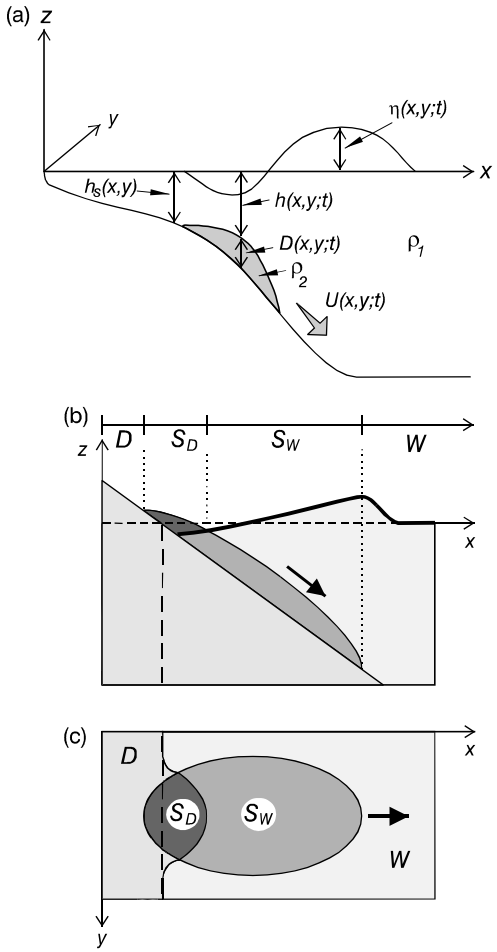


*Figure 1. (a) Sketch of a submarine landslide with density $\rho_2$, thickness D, and water depth h, and associated surface waves of height $\eta$. (b) Side view, and (c) plan view of a combined subaerial and submarine slide (see the text for description of the letters).*

$$U_m(x,y,z;t) = U(x,y;t)\left(2\xi - \xi^2\right), \tag{1a}$$

$$V_m(x,y,z;t) = V(x,y;t)\left(2\xi - \xi^2\right), \tag{1b}$$

where $\xi = (z + h_S)/D$. The equations for conservation of mass and momentum for a viscous submarine slide have the form [14]:

$$\frac{\partial D}{\partial t}+\frac{2}{3}\left[\frac{\partial (DU)}{\partial x}+\frac{\partial (DV)}{\partial y}\right]=0\ ; \tag{2}$$

$$\rho_2\frac{2}{3}\left[\frac{\partial U}{\partial t}-\frac{1}{5}\frac{U}{D}\frac{\partial D}{\partial t}+\frac{4}{5}\left(U\frac{\partial U}{\partial x}+V\frac{\partial U}{\partial y}\right)\right]=-g\left[(\rho_2-\rho_1)\left(\frac{\partial D}{\partial x}-\frac{\partial h_s}{\partial x}\right)+\rho_1\frac{\partial \eta}{\partial x}\right]-\frac{2\mu U}{D^2}\ ; \tag{3a}$$

$$\rho_2\frac{2}{3}\left[\frac{\partial V}{\partial t}-\frac{1}{5}\frac{V}{D}\frac{\partial D}{\partial t}+\frac{4}{5}\left(U\frac{\partial V}{\partial x}+V\frac{\partial V}{\partial y}\right)\right]=-g\left[(\rho_2-\rho_1)\left(\frac{\partial D}{\partial y}-\frac{\partial h_s}{\partial y}\right)+\rho_1\frac{\partial \eta}{\partial y}\right]-\frac{2\mu V}{D^2}. \tag{3b}$$

The continuum equation (2) is the same as in the JLB94 model. However, the momentum equations (3a) and (3b) are slightly different from those presented by *Jiang and LeBlond* [1] as a result of corrections we have made to several of the constant coefficients in the terms in the square brackets on the left-hand sides of these equations. Numerical experiments we have conducted show that the small errors in these advective terms in the JLB94 model may cause 20-25% errors in computed tsunami heights.

For a subaerial slide, it is useful to introduce a new variable, $h_w$, the full water thickness $(h_w=\eta+h=\eta-D+h_s)$, and to present equations (3a) and (3b) in the form:

$$\rho_2\frac{2}{3}\left[\frac{\partial U}{\partial t}-\frac{1}{5}\frac{U}{D}\frac{\partial D}{\partial t}+\frac{4}{5}\left(U\frac{\partial U}{\partial x}+V\frac{\partial U}{\partial y}\right)\right]=-g\left[\rho_2\left(\frac{\partial D}{\partial x}-\frac{\partial h_s}{\partial x}\right)+\rho_1\frac{\partial h_w}{\partial x}\right]-\frac{2\mu U}{D^2}; \tag{4a}$$

$$\rho_2\frac{2}{3}\left[\frac{\partial V}{\partial t}-\frac{1}{5}\frac{V}{D}\frac{\partial D}{\partial t}+\frac{4}{5}\left(U\frac{\partial V}{\partial x}+V\frac{\partial V}{\partial y}\right)\right]=-g\left[\rho_2\left(\frac{\partial D}{\partial y}-\frac{\partial h_s}{\partial y}\right)+\rho_1\frac{\partial h_w}{\partial y}\right]-\frac{2\mu V}{D^2}. \tag{4b}$$

For the subaerial zone, $S_D$, we have the particular case of zero water thickness, $h_w=0$, for which equations (4a) and (4b) describe slide motion on a dry coast.

The above equations are solved subject to the condition of zero transport through the coastal boundary ($G$) and require that the slide does not cross the outer (open) boundary ($\Gamma$). The condition of no volume transport through the coast gives

$$U_n=0 \qquad \text{on } G, \tag{5}$$

where $U_n$ is the normal slide velocity. The initial slide has a rectangular bottom periphery oriented at a given angle $\beta$ and, as noted above, is assumed to have a parabolic cross-section.

## 2.2. RIGID-BODY SLIDE

The rigid-body model assumes that the shape and dimensions of the initial slide remain invariant during the slide motion. All points of the rigid body move with the same velocity $\mathbf{U}=\mathbf{U}(t)$ and the position of the slide changes with time through the relation:

$$D(x,y;t)=D_0\big(x-X(t),y-Y(t)\big), \tag{6}$$

where $D_0$ is the initial slide distribution, and $X=\int_0^t U dt$, $Y=\int_0^t V dt$. In solving the

equations of motion, we further assume that: (1) Bottom friction on the slide is proportional to the normal pressure, *P*; (2) there are no hydraulic forces ("form drag") on the slide; and (3) the bottom slope is small, $|\nabla h| << 1$. Under these assumptions, the momentum equation of the slide becomes

$$\rho_2 \frac{d\mathbf{U}}{dt} \iint_S D ds = \nabla h \cdot P - k \frac{\mathbf{U}}{|\mathbf{U}|} P \ , \tag{7}$$

where *k* is the nondimensional coefficient of kinetic friction (the Coulomb friction coefficient), *S* is the surface area of the slide,

$$P = g \iint_S (\rho_1 \eta + \Delta\rho D) ds \ , \tag{8}$$

and $\Delta\rho = \rho_2 - \rho_1$ is the density difference between the slide and seawater. The boundary conditions for the rigid slide are the same as for the viscous slide.

## 2.3. SURFACE WAVES

For surface waves generated by a submarine slide, the water motions are nearly horizontal and the pressure is hydrostatic (long-wave approximation). The nonlinear shallow-water equations then have the form [1,15]:

$$\frac{\partial h_w}{\partial t} + \frac{\partial (h_w u)}{\partial x} + \frac{\partial (h_w v)}{\partial y} = 0; \tag{9}$$

$$\frac{\partial u}{\partial t} + u\frac{\partial u}{\partial x} + v\frac{\partial v}{\partial y} = -g\frac{\partial \eta}{\partial x}; \tag{10a}$$

$$\frac{\partial v}{\partial t} + u\frac{\partial v}{\partial x} + v\frac{\partial v}{\partial y} = -g\frac{\partial \eta}{\partial y}, \tag{10b}$$

which are applicable to wet zones, $S_W$ and $W$ (see Figure 1c). At the shore (boundary *G*), we assume a vertical wall with zero normal velocity:

$$u_n = 0 \qquad \text{on } G. \tag{11}$$

At the open boundary ($\Gamma$), the one-dimensional radiation condition for outgoing waves is:

$$\frac{\partial \eta}{\partial t} = \operatorname{sgn}\left(\frac{\partial \eta}{\partial t}\right) \sqrt{gh - \left[\left(\frac{\partial \eta}{\partial x}\right)^2 + \left(\frac{\partial \eta}{\partial y}\right)^2\right]} \tag{12}$$

At the initial time, *t* = 0, both the slide and the sea surface are at rest.

## 2.4. MODEL APPROACH

To solve equations (2)-(4), (7)-(8), and (9)-(10) with boundary conditions (5) and (11)-(12), we used an explicit finite-difference method with the Arakawa C-grid approximation. Velocity computational nodes are shifted by one-half the time and space steps relative to the sea level and slide-water interface computational nodes (the so-called staggered leap-frog scheme [23]). To avoid generation of erroneous small-scale oscillations, the time step ( $\Delta t$ ) was taken to be 1/3-1/5 the value required for the Courant stability criterion. To suppress numerical instability, the advective terms in equations (4) and (10) were represented through the upstream approximation scheme [24, 25]. For a detailed description of the present numerical model, the reader is directed to [15].

As previously emphasized, the main problem with numerical simulating subaerial slides is that the wet and dry areas change during the slide/wave motions, creating a variable boundary between the two areas. This is a well-known problem in tsunami run-up studies [23]. The drying of the wet area is not overly complicated. Here, the rule is that if the water thickness becomes equal to or less than zero, the respective point is assumed to be dry. Flooding of the dry area is a more serious problem. To describe the nonlinear interaction between the moving subaerial landslide and the overlying water, we have used the method proposed by *Titov and Synolakis* [26]. In this case, the wet boundary is determined as the intersection of the coastal slope and the horizontal plane of the sea level at the last "wet" point. When sea level at a "dry" point becomes higher than the fixed coastal elevation, this point is assumed to become "wet". This method is more stable to depth and coastline irregularities than other methods. A more detailed discussion of the of the "wetting" and "drying" problem in the area of the landslide using the present numerical algorithm is given by [15]

## 2.5. NONDIMENSIONAL VARIABLES

Following *Jiang and LeBlond* [1, 13], we have used nondimensional variables in our numerical experiments. We chose the initial maximum slide thickness, $D_0$, as the vertical length scale, the initial slide length, $L$, as the horizontal length scale, and $t_0 = (D_0 / g)^{1/2}$ as the time scale. The horizontal velocities are normalized using $U_0 = L_0 / t_0$. Thus, we adopt the following nondimensional variables:

$$(x', y') = (x, y) / L; \tag{13a}$$

$$(h', D', \eta') = (h, D, \eta) / D_0; \tag{13b}$$

$$t' = t / t_0; \qquad t_0 = (D_0 / g)^{1/2}; \tag{13c}$$

$$(u', v', U', V') = (u, v, U, V) / U_0; \qquad U_0 = L / t_0. \tag{13d}$$

The energy of the slide and generated surface waves are normalized as:

$$E' = E / E_0; \qquad E_0 = \frac{\rho_2 g L^2}{D_0}. \tag{14}$$

Nondimensional variables are used in Figures 2-7.

## 3. Wave Evolution

The two models described above were used to study water waves generated by landslides on a gentle uniform slope in shallow water. We first examined some general properties of tsunami waves generated by both rigid-body and viscous slides. Figures 2 and 3 present results for these models for subaerial and submarine slides. The computations have been made for slide density $\rho_2$ = 2.0 g·cm$^{-3}$ for both slides, Coulomb friction coefficient $k$ = 0.02 (for the rigid-body slide), and kinematic viscosity coefficient $\nu = \mu / \rho_2$ = 0.01 m$^2$s$^{-1}$ (for the viscous slide). The general results are similar for both models and correspond well to those obtained by previous investigators [27, 19, 1, 13]. In particular, the slide moving into deeper water forms a crest wave propagating ahead of the slide with a wave trough following the crest. However, there are some important differences between the rigid-body and viscous models, and between subaerial and submarine landslides. The principal difference is that a rigid-body slide produces much higher waves than a viscous slide, indicating that a rigid-body slide is a much more efficient tsunami wave generator than a viscous slide. Similarly, subaerial slides are much more efficient wave generators than purely submarine slides (Figures 4 and 5).

A subaerial slide entering the water brings an additional volume causing a respective displacement of the sea surface. Therefore, the initial wave crest is sufficiently larger than the following wave trough (Figure 4). *Heinrich* [19] obtained similar results both in laboratory modeling of a subaerial solid triangle block sliding freely downslope into the water and by corresponding numerical computations. *The added volume displacement of the water is one of the reasons why subaerial slides generate significantly larger surface waves than submarine landslides.*

For a submarine slide, three major waves are produced (Figure 5): (1) The leading wave crest propagating rapidly offshore ahead of the moving slide with shallow-water wave speed $c = \sqrt{gh}$ ; (2) the wave trough propagating offshore with the speed of the slide; and (3) the wave trough propagating shoreward. Similar results were obtained by *Heinrich* [19] and *Jiang and LeBlond* [1, 13]. For a rigid-body slide, the second wave, which is bound to the slide as a forced wave, is significantly larger than two other generated waves (Figure 5a); for a viscous slide all three waves have comparable heights (Figure 5b). An important aspect of this process is that, due to amplitude dispersion, the viscous slide forms a bore-like leading edge with a steep frontal wall as it moves downslope (Figure 3; see also Figures 3-8 in [13]). This frontal bore in the slide gives rise to a corresponding bore-like negative surface wave propagating with the frontal speed of the slide (Figure 5b).

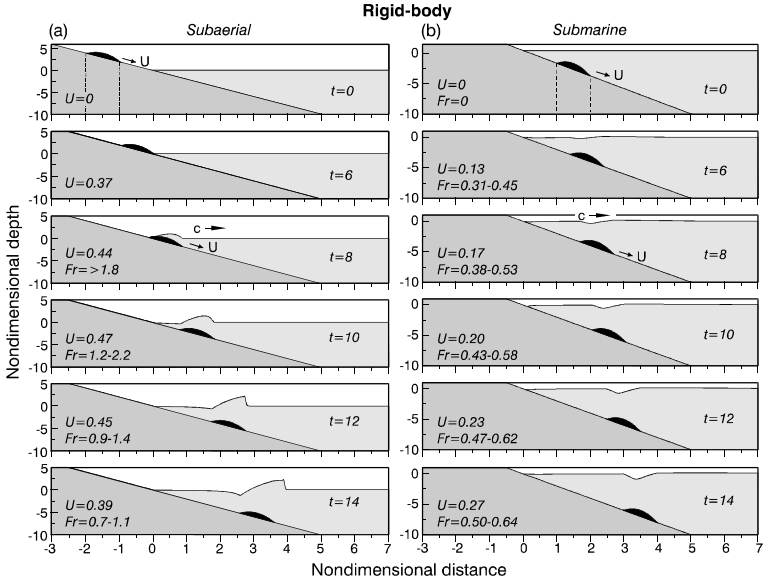


*Figure 2. Tsunami waves generated by a rigid-body slide moving downslope at speed U (slope angle $\psi$ = 4°, slide density $\rho_2$ = 2.0 g·cm$^{-3}$, friction coefficient k = 0.02). (a) Subaerial slide; (b) submarine slide. Nondimensional time, t, slide speed, U, and Froude number, Fr=U/c, where $c=\sqrt{gh}$ is the long-wave speed, are presented in the plots.*

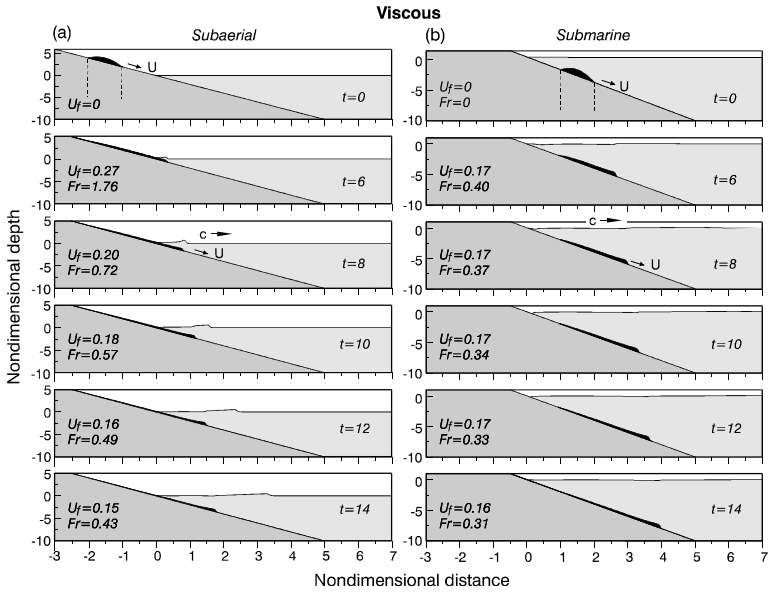


*Figure 3. The same as in Figure 2 but for a viscous slide with kinematic viscosity $\nu$ = 0.01 m$^2$·s$^{-1}$.*

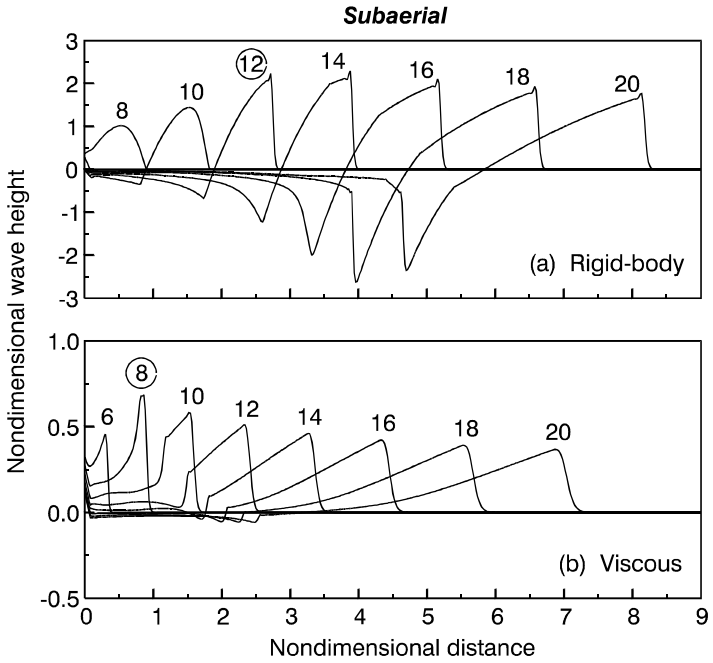


*Figure 4. Tsunami waves for fixed times generated by a subaerial slide: (a) A rigid-body slide, and (b) a viscous slide. Parameters of the slides are the same as in Figures 2 and 3. Note that the wave-height scale for the viscous model is four times greater than for the rigid-body model. The circled times are the times closest to resonance (Fr = 1.0).*

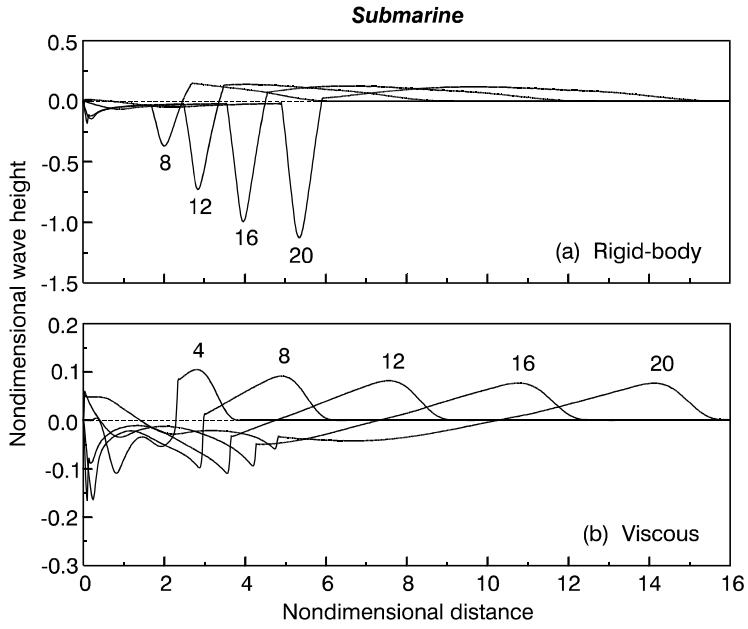


*Figure 5. The same as in Figure 4 but for tsunami waves generated by a purely submarine slide.*

## 4. Slide/Wave Speed and Froude Number

The character and intensity of the tsunami waves, as well as the coupling between the slide and the waves, strongly depends on the Froude number, *Fr* (the ratio between the slide and wave speeds). Resonance occurs when these speeds are equal; i.e. when *Fr* = 1.0.

For a rigid-body, which moves as an entity with the same speed *U*, the Froude number can be defined as

$$Fr = U / c\,, \tag{15a}$$

where $c = \sqrt{gh(x, y)}$ is the local long-wave speed. In contrast, different parts of a viscous slide move with different speeds. For the latter case, we may define the Froude number as

$$Fr = U_f/c, \tag{15b}$$

where $U_f$ is the speed of the slide front [13]. Figures 2 and 3 show the values of $U$ ($U_f$) and corresponding *Fr*. Because the depth is different near the front and the rear of the rigid-body slide, the wave speed, *c*, and Froude number are also different (Figure 2). For the viscous slide (Figure 3), the values of $U_f$ and *Fr* are presented for the front slide point.

The Froude number for submarine landslides plays the same role as the Mach number for high-speed aircraft. As seen from Figure 2a, the character of the water disturbances is significantly different for "super-sonic" (*Fr* > 1.0) and "sub-sonic" (*Fr* < 1.0) slide motions. The super-sonic slide movement (*Fr* > 1.0) does not induce free-propagating water waves so that the water displacement (forced wave) is locked to the slide and moves with the slide speed, almost duplicating its form. When the slide thickness is much smaller than the water depth, we can describe this forced wave roughly as

$$\eta \approx \frac{DU^2}{U^2 - c^2} \tag{16}$$

Expression (16) is similar to well-known "Proudman expression" for cyclone-induced displacements of sea level [28]. For super-sonic slide motion (when $U > c$ and *Fr* > 1.0) the forced wave is positive (crest), whereas for sub-sonic slide motion ($U < c$ and *Fr* < 1.0) it is negative (trough) (Figures 2 and 3).

As shown by our numerical experiments, an initially subaerial rigid-body slide moving underwater downslope spans three consecutive regimes (Figures 2a and 4a):

(1) *Super-sonic* (*Fr* > 1.0): There is only one wave, the positive forced wave (crest), which repeats the form of the slide and moves together with it.

(2) *Resonant* (*Fr* ~ 1.0): The height of the positive forced wave is significantly amplified (crest maximum is about $2.5D_0$) and the frontal side of the wave becomes very steep forming a bore. In the rear of the slide an intensified negative (trough) wave forms.

(3) *Sub-sonic* (*Fr* < 1.0): The first (crest) wave becomes free and propagates away rapidly from the slide with the long-wave speed $c = \sqrt{gh}$, its height decreasing with distance. In contrast, the second (trough) wave is a forced wave, bound to the slide motion, its height slowly decreasing with time.

A subaerial viscous slide moving underwater has the same three regimes as the rigid-body slide above, except that surface wave generation is now less efficient and of a more complex nature (Figures 2b and 4b). The tsunami waves for a viscous slide are induced in three different ways: By the initial water displacement by the slide, by propagation of the

slide front, and by underwater changes in the slide configuration.

In all our experiments, *purely submarine slides* (both rigid-body and viscous) were "sub-sonic" (see Figure 3 as an example) and the Froude numbers were always significantly smaller than unity. This result follows from the general properties of underwater slide motions [22, 29]. More specifically, the speed of an underwater rigid-body sliding down a gentle slope may be approximated from the equation:

$$\rho_2 \frac{U^2}{2} + gk(\rho_2 - \rho_1)(x - x_0) = g(\rho_2 - \rho_1)(h - h_0), \tag{17}$$

where $x_0$ and $h_0$ are the initial slide position and water depth, and $x$ and $h$ are the current position and depth. This yield,

$$U = \left[ 2g \frac{\rho_2 - \rho_1}{\rho_2} [h - h_0 - k(x - x_0)] \right]^{1/2} \tag{18a}$$

for the slide speed and

$$Fr = \frac{U}{c} = \left[ \frac{2g \frac{\rho_2 - \rho_1}{\rho_2} [h - h_0 - k(x - x_0)]}{gh} \right]^{1/2} = \left[ 2 \frac{\rho_2 - \rho_1}{\rho_2} \left( 1 - \frac{h_0}{h} - k \frac{x - x_0}{h} \right) \right]^{1/2} \tag{18b}$$

for the Froude number.

The fastest slide speed for submarine slides is achieved when a slide starts from the coastline $(h_0 = 0, \quad x_0 = 0)$. Equation (18a) in that case has the form

$$U = \left[ 2g \frac{\rho_2 - \rho_1}{\rho_2} (h - kx) \right]^{1/2}, \tag{19a}$$

and equation (18b) becomes

$$Fr = \frac{U}{c} = \left[ 2 \frac{\rho_2 - \rho_1}{\rho_2} \left( 1 - k \frac{x}{h} \right) \right]^{1/2}. \tag{19b}$$

Typical density values for natural alluvial and deluvial sediments are $\rho_2$ = 1.2-2.0 g·cm$^{-3}$ [13]. Assuming a water density $\rho_1 \approx$ 1.0 g·cm$^{-3}$, it follows from expressions (19a) and (19b), that if $\rho_2 \leq$ 2.0 g·cm$^{-3}$ then $U < c$, and $Fr < 1.0$ always. Actual Froude numbers will be even smaller because: (1) Expressions (18) and (19) do not take into account hydraulic resistance to slide motion, which would reduce the slide speed[1]; and (2) more realistic deeper initial source areas will reduce the slide speed. We therefore conclude that, for natural submarine landslides, *resonance coupling of slides and surface waves is impossible*. Resonance can occur only if $\rho_2 >$ 2.0 g·cm$^{-3}$ (i.e. for strongly consolidated sediments or rock) or if the slide starts above the water. *Existence of the resonance regime for subaerial slides and absence of this regime for purely submarine slides is a second reason why*

[1] The influence of water resistance on slide speed and Froude number is discussed by *Harbitz* [22] and *Pelinovsky and Poplavsky* [29], among others.

*subaerial slides are much more efficient tsunami generators than submarine slides.*

## 5. Energy Estimates

The numerical experiments described above enable us to derive relative energy estimates of the generated tsunami waves. Multiplying equation (9) by $g\eta$, (10a) by $h_w u$, and (10b) by $h_w v$, and summing all three contributions, gives the time rate of change of total wave energy, $\frac{\partial \varepsilon}{\partial t}$:

$$\frac{\partial \varepsilon}{\partial t} = g\eta \frac{\partial D}{\partial t} - \frac{\partial}{\partial x}(h_w u \varepsilon_0) - \frac{\partial}{\partial y}(h_w v \varepsilon_0), \tag{20}$$

where $\varepsilon = \frac{1}{2}(h_w u^2 + h_w v^2 + g\eta^2)$ and $\varepsilon_0 = \frac{1}{2}(u^2 + v^2 + 2g\eta)$. Integration of (20) over the area, $\Omega$, occupied by the waves and slide yields,

$$\frac{\partial E}{\partial t} = \iint_{\Omega} g\eta \frac{\partial D}{\partial t} ds - \int_{\Gamma} \varepsilon_0 h_w u_n dl, \tag{21}$$

where $\Gamma$ is the open boundary, $u_n$ is the current velocity component normal to this boundary, and $E = \iint_{\Omega} \varepsilon ds$ is the wave energy. Equation (21) has a simple interpretation: changes in wave energy in the tsunami domain are the sum of the wave generation within the domain and the energy flux through the open boundary. The first term in the right side of (21)

$$W = \iint_{\Omega} g\eta \frac{\partial D}{\partial t} ds \tag{22}$$

describes the rate-of-energy-generation (energy generated in the area, $\Omega$, per unit time).

Figure 6 presents numerical estimates for the rate-of-energy-generation as a function of time for subaerial and submarine slides moving downslope. Here, the curves (solid lines) give the relative transfer of energy from the slide motion into the surface waves at different time and slides positions/depth. Also shown are the corresponding changes in Froude number. There is clearly good agreement between the two properties for subaerial slides, with sharp resonant peaks in the rate-of-energy transfer corresponding to *Fr* = 1.0 (Figure 6a,b). The small temporal shift in the resonance peak for the viscous subaerial slide arises from the fact that the maximum thickness of the slide lags a little behind the leading edge of the slide (the point at which the Froude number is estimated).

There also is a good correlation between Froude number and rate-of-energy-generation for submarine slides (Figure 6c, d). For example, the time of maximum rate-of-energy-

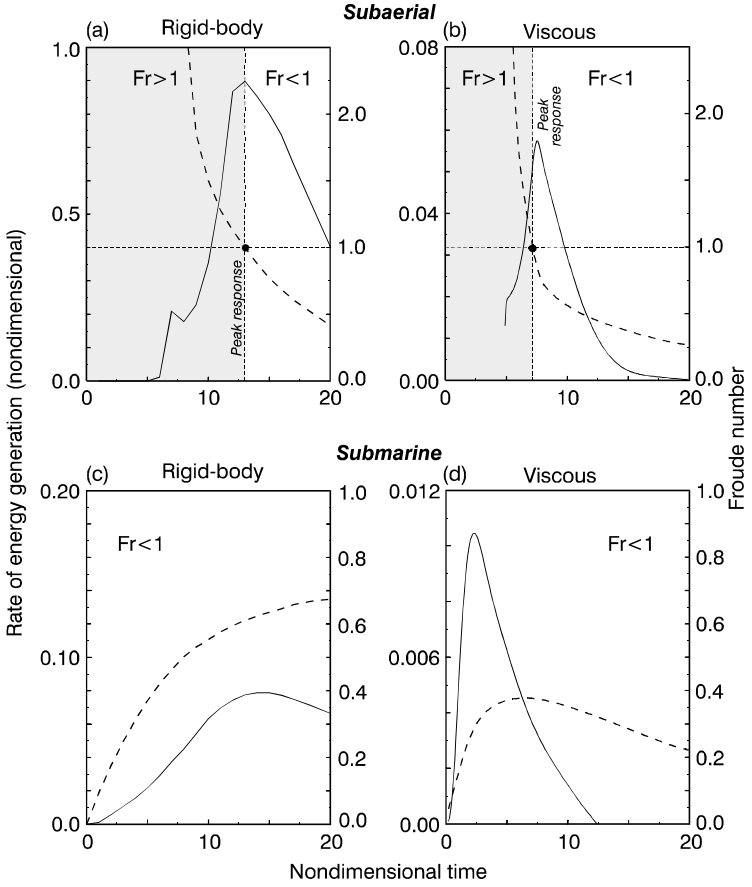


*Figure 6. Rate-of-energy-generation (solid lines) as a function of nondimensional time for four slide models: (a) Rigid-body, subaerial; (b) viscous, subaerial; (c) rigid-body, submarine; and (d) viscous, submarine. Dashed lines show variations in the accompanying Froude number. Slope angle is* $\psi$ *= 4°, slide density* $\rho_2$ *= 2.0 g·cm$^{-3}$, friction coefficient k = 0.02 (for a rigid-body slide) and kinematic viscosity* $\nu$ *= 0.01 m$^2$·s$^{-1}$ (for a viscous slide).*

generation for the viscous submarine slide occurs very close to the time of maximum Froude number ($Fr$ = 0.45) (Figure 6d). The rate-of-energy-generation for the rigid-body submarine slide increases with increasing $Fr$. This effect is somewhat hidden by changes in water depth which also have an important impact on wave generation, with wave generation decreasing with increasing depth. As a consequence, the rate-of-energy-generation has a maximum at $t$ = 13 (Figure 6c) despite the fact that $Fr$ keeps increasing for an infinite slope.

## 6. Influence of Initial Slide Conditions

It is instructive to examine the effect of initial slide position (i.e. height above sea level for subaerial slides or water depth for submarine slides) on surface wave generation. Results from numerical experiments for various slope angles for rigid-body and viscous models were surprisingly different (Figure 7). For a rigid-body slide, the greater the initial slide height above sea level, the more energetic the generated tsunami waves (Figure 7a).

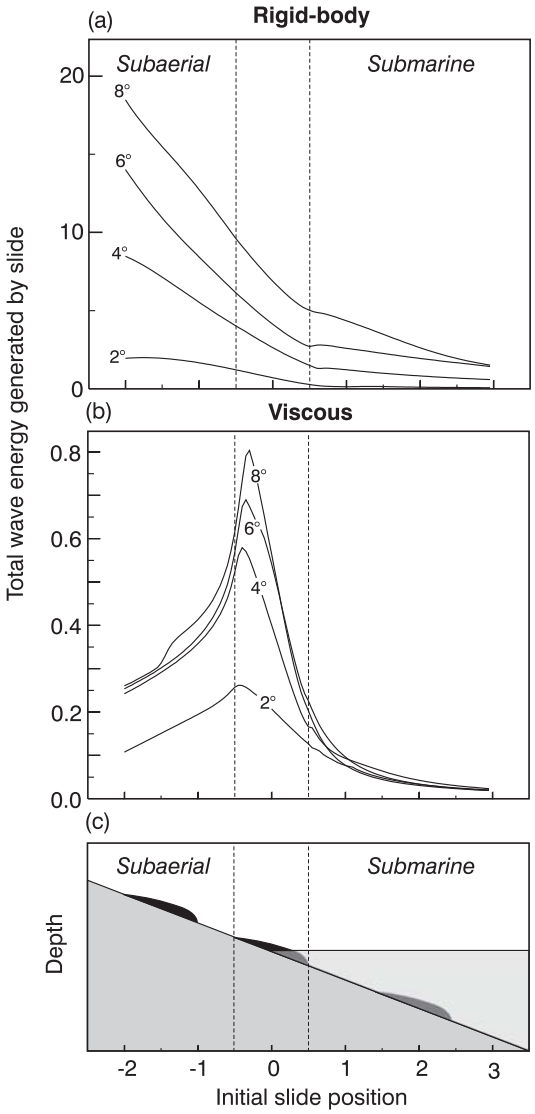


*Figure 7. Total wave energy as functions of slope angle and the initial slide position for: (a) A rigid-body slide; and (b) a viscous slide. The initial slide positions are shown in (c). Parameters of the slides are the same as in Figure 6.*

This result is in agreement with laboratory and computational results by *Watts* [30, 31] who demonstrated that rigid-body landslide generated tsunamis have amplitudes proportional to their vertical center of mass displacement. For viscous slides, there is an optimal slide position (height), located close to the coastline, which produces the largest tsunami waves. Slides initially located above or below this position generate less energetic waves (Figure 7b).

Our experiments with slope angles in the range from 2° to 10° for both models (rigid-body and viscous) gave identical results: The steeper the slope, the higher the generated surface waves. In general, the energy of the generated tsunami waves for this range of slope angles is roughly proportional to the angle. Thus, a change of angle from 2° to 8° increases the surface wave energy by a factor of four (Figure 7).

## 7. Discussion

We have conducted a suite of numerical simulations to compare tsunami wave generation by rigid-body and viscous slides and to examine the relative contributions from the subaerial and submarine components of these slides. The numerical experiments reveal significant differences in the computed wave heights for the rigid-body and viscous models. Specifically, for slides with the same initial position and shape, the rigid-body slide model produces surface waves which are roughly a factor of four higher than waves produced by the viscous slide model[2]. Both models were carefully tested, the rigid-body model being verified against analytical computations, and the viscous model compared with the results of *Jiang and LeBlond* [1, 13]. Model differences are therefore considered to be physical rather than mathematical. The models were equivalent in almost all aspects, except that the rigid-body slide treats the slide as an undeformable solid body, while the viscous model allows the slide to deform as a viscous fluid[3].

It is clear from our study that rigid-bodies are much more efficient tsunami generators than viscous slides. What is important to understand is which model is more *physically realistic* and therefore better to describe actual slide failure events. There are at least two key scientific aspects to be addressed when discussing this problem: (1) The accurate numerical modeling of historical slide-generated tsunamis; and (2) the estimation of tsunami risk for coastal areas with the potential for submarine and subaerial slides.

Use of the rigid-body model of submarine slides has a long history. Some simple estimates for this model may be obtained analytically [29, 30, 31]. Laboratory modeling of slide-generated waves also mainly deals with rigid bodies, which can then be compared with analytical or numerical solutions [27, 19, 30, 31]. On this basis, it makes sense that use of the rigid-body model has been so widespread and that the majority of publications examining slide-generated tsunamis are based on this approximation. Unfortunately, most

[2] These estimates pertain to the forward (offshore) propagating waves in Figures 4 and 5; the differences in wave heights for backward (onshore) propagating waves (i.e. run-up heights) for these models are considerably smaller.

[3] *Watts et al.* [32] compared rigid-body and viscous slide models and found that the former model generates higher surface waves than the latter; however, in their case the difference was much smaller than in ours, probably because parameters of their models were fitted to reduce this difference. In addition, their rigid-body model was simply a boundary element model for potential flow, and their viscous model a shallow-water two-layer model similar to JLB94.

geotechnical information for land and marine slides, slumps, avalanches, and rock falls indicate that the rigid-body approximation is too simplistic and that the viscous fluid model better describes these processes [33]. For this reason, the viscous fluid slide model, first rigorously formulated by *Jiang and LeBlond* [1, 13], is now widely used to simulate catastrophic tsunamis arising from submarine landslides. Examples include Nice, France (1979) [18], Skagway (1994) [14, 8, 15], and PNG (1999) [4, 16, 17]. In all of the above events, the viscous model gives reasonable agreement with the existing empirical data.

The consistency between the observed tsunami waves and numerical simulations of these waves using the viscous slide model implies that this is the preferred model for determining landslide-generated tsunami risk along the coast (i.e. possible tsunami heights which could be caused by potential submarine or subaerial landslides). Long-term tsunami prediction in coastal regions ("tsunami-zoning") is a key problem for hazard mitigation and long-term planning, and is also a necessary element of any planning for new construction in the coastal zone [34,35]. A common argument is that a rigid-body model produces higher tsunami waves, so this model should be used for estimation of tsunami risk. We disagree with this notion. As the present results indicate, the rigid-body model strongly overestimates actual tsunami heights. If accepted for engineering design, such overestimation could greatly increase construction costs. There are no perfect models. Nevertheless, it is important to use the *best available science* for tsunami predictions [*Frank González*, Pers. Comm.]. In our opinion, the results from the viscous slide model are more realistic than those from the rigid-body model, making the viscous model the model of choice.

Another important consideration is the influence of the subaerial component of landslides on tsunami generation. Although most existing models omit this component of the slide, our study demonstrates that it is of primary importance. There are two fundamental effects associated with this component: (1) The subaerial component of the slide adds an additional volume to the ocean, causing a corresponding displacement of the sea surface; and (2) there is always a point (in time and space) where $Fr = 1.0$ for which there is a resonant transfer of energy from the slide into the surface waves. In contrast, for purely submarine slides with $\rho_2 \leq 2.0$ g·cm$^{-3}$, the Froude number is always less than unity and resonance coupling of slides and surface waves is physically impossible (at least on Earth). Due to these two effects, subaerial slides are much more efficient tsunami generators than submarine slides. The catastrophic consequences and destructive waves associated with a relatively small slide failure in 1994 in Skagway Harbor were apparently initiated by the subaerial component of the slide. Incorporating this component into existing models is essential for correct representation of natural events.

For subaerial slides, the energy of the generated tsunami waves strongly depends on the initial slide height above sea level. Rigid-body subaerial slides with higher initial elevations generate larger tsunami waves because their potential energy is greater, resulting in more energy being transferred into the surface waves (for similar reasons, earthquakes of larger magnitude generally produce higher tsunamis). However, for viscous slides there is an additional opposing effect. Because different parts of a viscous slide move with different velocities, the slide stretches and spreads during its movement downslope, forming a long sediment tail (see Figure 3). As a consequence, the tsunami-generating efficiency of the slide is reduced. The greater the distance traveled by the slide, the more pronounced is this effect. The existence of an optimal subaerial point (slide height) associated with maximum generated tsunami waves is apparently the direct consequence of these two opposing effects.

## 8. Conclusions

The findings of our numerical simulations can be summarized in point form as follows:

(1) A rigid-body slide has greater tsunami-generating efficiency and produces much higher tsunami waves than a viscous (liquid) slide. The choice of "most realistic" slide model should be a physical, rather than a mathematical, consideration. We argue that, in most cases, the viscous slide model is the model of choice.

(2) The maximum wave height and energy of generated surface waves depend on various slide parameters and factors, including: Slide volume, type of slide (viscous or rigid), slide density, slide position (relative height or depth), and slope angle. For a rigid-body slide, the higher the initial slide above sea level, the higher the generated waves. For a viscous slide, there is an optimal slide position (height), located close to the shore, which produces the largest tsunami waves. Slides initially located above or below this position generate less energetic waves. An increase in slide volume, density, and slope angle always increases the energy of the generated waves.

(3) The added volume that occurs when a subaerial slide enters the water results in a displacement of the sea surface and a significant increase in height of the leading wave crest.

(4) The critical parameter determining the generation of surface waves is the Froude number (the ratio between the slide and wave speeds). The most efficient generation occurs near resonance when $Fr$ = 1.0. For purely submarine slides with water density $\rho_1$ ~ 1.0 g·cm$^{-3}$ and slide density $\rho_2 \leq$ 2.0 g·cm$^{-3}$, the Froude number is always less than unity and resonance coupling of slides and surface waves is physically impossible. For subaerial slides there is always a resonant point (in time and space) where $Fr$ = 1.0 for which there is a significant transfer of energy from a slide into surface waves. This effect, combined with the displacement of the sea surface (point 3, above), are the two main reasons that subaerial slides are much more important for tsunami generation than submarine slides.

## Acknowledgements

The authors thank Patricia Kimber for drafting the figures. This research was partially sponsored by INTAS project 99-1600.

## References

1. Jiang, L. and LeBlond, P.H.: 1994, Three-dimensional modeling of tsunami generation due to a submarine mudslide, *J. Phys. Oceanogr.* **24** (3), 559-572.
2. Imamura, F., and Gica, E.C.: 1996, Numerical model for tsunami generation due to subaqueous landslide along a coast, *Science of Tsunami Hazards* **14** (1), 13-28.
3. Tappin, D. et al.: 1999, Sediment slump likely caused 1998 Papua New Guinea tsunami, *EOS* **80**, 329, 334, 340.
4. Heinrich, P., Piatensi, A., Okal, E., and Hébert, H.: 2000, Near-field modeling of the July 17, 1998 tsunami in Papua New Guinea, *Geophys. Res. Let.* **27**, 3037-3040.
5. Altinok, Y., Alpar, B., Ersoy, S. and Yalciner, A.C.: 1999, Tsunami generation of the Kocaeli Earthquake (August 17$^{th}$, 1999) in the Izmit Bay: Coastal observations, bathymetry and seismic data, *Turkish J. Marine*

*Sciences* **5** (3), 131-148.
6. Kulikov, E.A., Rabinovich, A.B., Thomson, R.E., and Bornhold, B.D.: 1996, The landslide tsunami of November 3, 1994, Skagway Harbor, Alaska, *J. Geophys. Res.* **101** (C3), 6609-6615.
7. Kowalik, Z.: 1997, Landslide-generated tsunami in Skagway, Alaska, *Science of Tsunami Hazards* **15** (2), 89-106.
8. Rabinovich, A.B., Thomson, R.E., Kulikov, E.A., Bornhold, B.D., and Fine, I.V.: 1999, The landslide-generated tsunami of November 3, 1994 in Skagway Harbor, Alaska: A case study, *Geophys. Res. Let.* **26**, (19), 3009-3012.
9. LeBlond, P.H. and Jones, A.T.: 1995, Underwater landslides ineffective at tsunami generation, *Science of Tsunami Hazards* **13** (1), 25-26.
10. Miller, D.J.: 1960, The Alaska Earthquake on July 10, 1958: Giant wave in Lituya Bay, *Bull. Seism. Soc. America* **50** (2), 253-266.
11. Lander, J.F.: 1996, *Tsunamis Affecting Alaska, 1737-1996*. Boulder, US Dep. Comm., 195 p.
12. Raichlen, F., J.J. Lee, C. Petroff, and P. Watts, 1996: The generation of waves by a landslide: Skagway, Alaska: A case study, *Proc. 25th Coastal Eng. Conf.*, ASCE, Orlando, Florida, 1478-1490.
13. Jiang, L. and LeBlond, P.H.: 1992, The coupling of a submarine slide and the surface waves which it generates, *J. Geophys. Res.* **97** (C8*)*, 12,731-12,744.
14. Fine, I.V., Rabinovich, A.B., Kulikov, E.A., Thomson, R.E., and Bornhold, B.D.: 1998, Numerical modelling of landslide-generated tsunamis with application to the Skagway Harbor tsunami of November 3, 1994, *Proc. Int. Conf. on Tsunamis*, Paris, 211-223.
15. Thomson, R.E., Rabinovich, A.B., Kulikov, E.A., Fine, I.V., and Bornhold, B.D.: 2001, On numerical simulation of the landslide-generated tsunami of November 3, 1994 in Skagway Harbor, Alaska, in *Tsunami Research at the End of a Critical Decade*, edited by G. Hebenstreit, Kluwer, Dorderecht, 243-282.
16. Titov, V.V., and González, F.: 2001, Numerical study of the source of the July 1998 PNG tsunami, in *Tsunami Research at the End of a Critical Decade*, edited by G. Hebenstreit, Kluwer, Dorderecht, 197-207.
17. Imamura, F., Hashi, K., and Imteaz, Md.M.A.: 2001, Modeling for tsunamis generated by landsliding and debris flow, in *Tsunami Research at the End of a Critical Decade*, edited by G. Hebenstreit, Kluwer, Dorderecht, 209-228.
18. Assier-Rzadkiewicz, S., Heinrich, P., Sabatier, P.C., Savoye, B., and Bourillet, J.F.: 2000, Numerical modelling of landslide-generated tsunami: The 1979 Nice event, *Pure Appl. Geophys.* **157**, 1707-1727.
19. Heinrich, P.: 1992, Nonlinear water waves generated by submarine and aerial landslides, *J. Waterways, Port, Coastal and Ocean Eng.*, ASCE, **118** (3), 249-266.
20. Heinrich, P., Mangeney, A., Guibourg, S., Roche, R., Boudon, G., and Vheminée, J.-L.: 1998, Simulation of water waves generated by a potential debris avalanche in Montserrat, Lesser Antilles, *Geophys. Res. Let.* **25** (19), 3697-3700.
21. Norem, H., J. Locat, and B. Schieldrop: 1991, An approach to the physics and modeling of submarine flowslides, *Mar. Geotechnol.* **9**, 93-111.
22. Harbitz, C.B.: 1992, Model simulations of tsunamis generated by the Storegga slides, *Marine Geology* **105**, 1-21.
23. Imamura, F.: 1996, Review of tsunami simulation with finite difference method, in *Long-Wave Runup Models*, edited by H. Yeh, P. Liu, and C. Synolakis, World Scientific, Singapore, 25-42.
24. Roache, P.J., 1976: *Computational Fluid Dynamics*, Hermosa Publ., Albuquerque, N.M., 446 p.
25. Mader, C.L.: 1988, *Numerical Modeling of Water Waves*, Univ. California Press, Berkeley.
26. Titov, V.V., and Synolakis, C.E.: 1998, Numerical modeling of tidal wave runup, *J. Waterw., Port, Coastal and Ocean Eng.,* ASCE, **124**, (3), 157-171.
27. Wiegel, R.L.: 1955, Laboratory studies of gravity waves generated by the movement of a submerged body, *Trans. Am. Geophys. Union* **36** (5), 759-774.
28. Proudman, J.: 1953, *Dynamic Oceanography*, Methuen and Co., London, 409 p.
29. Pelinovsky, E., and Poplavsky, A.: 1996, Simplified model of tsunami generation by submarine landslides, *Phys. Chem. Earth* **21** (12), 13-17.
30. Watts, P.: 1998, Wavemaker curves for tsunamis generated by underwater landslides, *J. Waterways, Port, Coastal and Ocean Eng.*, ASCE, **124** (3), 127-137.
31. Watts, P.: 2000, Tsunami features of solid block underwater landslides, *J. Waterways, Port, Coastal and Ocean Eng*., ASCE, **126**, (3), 144-152.
32. Watts, P., Imamura, F., and Grilli, S.: 2000, Comparing model simulations of three benchmark tsunami generation cases, *Science of Tsunami Hazards* **16** (2), 107-123.
33. Andresen, A., and Bjerrum, L.: 1967, Slides in subaqueous slopes in loose sand and silt, in *Marine Geotechnique*, edited by A.F. Richards, Univ. Illinois Press, Urbana, 221-239.

34. Chaudhry, M.H., Mercer, A.G., and Cass, D.: 1983, Modeling of slide-generated waves in a reservoir, *J. Hydr. Engin.*, ASCE, **109** (11), 1505-1520.
35. Mofjeld, H.O., González, F.I., and Newman, J.C.: 1999, Tsunami prediction in U.S. coastal regions, in *Coastal Ocean Prediction, Ch. 14, Coastal and Estuarine Studies 56* edited by C.N.K. Mooers, AGU, Washington, 353-375.